Food Chemistry 221 (2017) 1569–1577

Contents lists available at ScienceDirect

Food Chemistry

journal homepage: www.elsevier.com/locate/foodchem

Myricetin inhibits the generation of superoxide anion by reduced form of xanthine oxidase

Cen Zhang [a], Guowen Zhang [a,*], Yijing Liao [a], Deming Gong [b]

[a] State Key Laboratory of Food Science and Technology, Nanchang University, Nanchang 330047, China
[b] School of Biological Sciences, The University of Auckland, Auckland 1142, New Zealand

ARTICLE INFO

Article history:
Received 23 July 2016
Received in revised form 19 September 2016
Accepted 28 October 2016
Available online 31 October 2016

Keywords:
Myricetin
Xanthine oxidase
Superoxide anion
Inhibition
Molecular simulation

ABSTRACT

Myricetin, a plant-derived flavonol, was found to inhibit the formation of uric acid in a mixed-type manner with IC_{50} value of $(8.66 \pm 0.03) \times 10^{-6}$ mol L^{-1} and more potently inhibit the generation of superoxide anion (O_2^-) catalysed by xanthine oxidase (XOD) with IC_{50} value of $(4.55 \pm 0.02) \times 10^{-6}$ mol L^{-1}. Inhibiting O_2^- generation by myricetin may be attributed to the reduced form of XOD with a substantially higher reduction potential for FADH./$FADH_2$ couple. Moreover, molecular docking verified that myricetin bound to the site around isoalloxazine ring in the flavin adenine dinucleotide (FAD) domain to block the diffusion of O_2^- out of the FAD site, resulting in the transfer of another electron from $FADH_2$ to O_2^- to form hydrogen peroxide. This study has provided new insight into the role of myricetin in inhibiting XOD catalysis, which may be beneficial to improve myricetin's potential application in functional foods.

1. Introduction

Xanthine oxidase (XOD), which widely exists from bacteria to humans and in the various tissues of mammals, is a homodimer with a molecular mass of 290 kDa. Each subunit of XOD consists of an N-terminal domain with two iron sulfur centers, a central flavin adenine dinucleotide (FAD) cofactor, and a C-terminal molybdopterin domain containing the four redox centers aligned in an almost linear fashion (Enroth et al., 2000). XOD catalyses the oxidation of hypoxanthine and xanthine to uric acid in the metabolism of endogenous compounds such as purines. The hyperuricemia resulted from overproduction or underexcretion of uric acid is the critical cause of gout (Chu, Chen, Wu, & Hsieh, 2014). Recent study found that XOD might be associated with blood pressure regulation (Suzuki et al., 1998). The drugs targeting XOD have been usually used as effective treatments for gout in clinic.

Xanthine dehydrogenase (XDH), which can be readily converted to the oxidase form XOD by oxidation of sulfhydryl residues or by proteolysis, exhibits a preference for NAD^+ reduction at the FAD reaction site. Unlike XDH, XOD fails to react with NAD^+ and exclusively uses dioxygen as its substrate, generating superoxide anion (O_2^-) and hydrogen peroxide (Hille & Nishino, 1995). Previous studies have reported that excess generation of O_2^- led to many diseases and disorders, such as microbial infection, inflammation, hypertension and ischemia/reperfusion (I/R) injury (Fang et al., 2016). Intake of XOD inhibitors from foods may be a promising approach to preventing these diseases.

Although therapeutic agents allopurinol and newly licenced febuxostat have been commonly used for the treatment of hyperuricemia in clinic, severe side effects of these traditional agents aroused safety concerns, including bone marrow depression, hematological, hepatic, renal and gastrointestinal toxicities, and allergic reactions (Wang, Zhang, Pan, & Gong, 2015). Therefore, it is of necessity to find the efficient and less toxic XOD inhibitors for nutraceutical and pharmaceutical applications. As a group of natural products, flavonoid compounds have been found to possess many biological and pharmacological activities, such as antiviral, antibacterial, antioxidant activities, and inhibition of several enzymes (Romano et al., 2013). Amentoflavone and robustaflavone, isolated from selaginella tamariscina, were found to strongly inhibit XOD in a non-competitive manner with IC_{50} values of 3.02×10^{-5} and 2.23×10^{-5} mol L^{-1}, respectively (Wang, Liu et al., 2014; Wang, Curtis-Long et al., 2014). Nagao, Seki, and Kobayashi (1999) reported that chrysin was a potent inhibitor of XOD with an IC_{50} value of 5.02×10^{-6} mol L^{-1}. Fisetin was reported to significantly inhibit XOD activity and O_2^- generated by XOD with IC_{50} values of $(4.33 \pm 0.19) \times 10^{-6}$ mol L^{-1} and $(1.84 \pm 0.07) \times 10^{-6}$ mol L^{-1}, respectively (Cos et al., 1998).

* Corresponding author.
E-mail address: gwzhang@ncu.edu.cn (G. Zhang).

http://dx.doi.org/10.1016/j.foodchem.2016.10.136
0308-8146/

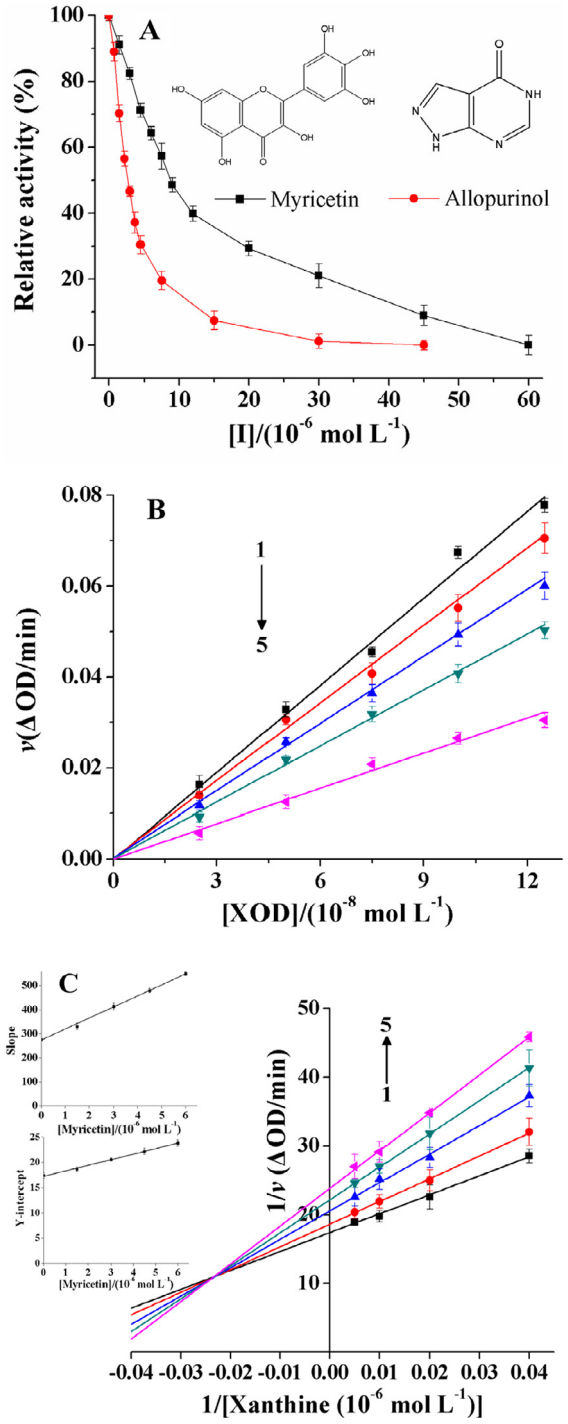

Fig. 1. (A) XOD activity in the absence and presence of myricetin and allopurinol at different concentrations (pH 7.4, T = 298 K). c(XOD) = 7.5×10^{-8} mol L^{-1}, and c (xanthine) = 5.0×10^{-5} mol L^{-1}. (B) Plots of v vs. [XOD]. c(xanthine) = 5.0×10^{-5} mol L^{-1}; c(myricetin) = 0, 1.5, 3.0, 4.5 and 9.0×10^{-6} mol L^{-1} for curves 1 → 5, respectively. (C) Lineweaver–Burk plots. c(XOD) = 7.5×10^{-8} mol L^{-1}; c(myricetin) = 0, 1.5, 3.0, 4.5 and 6.0×10^{-6} mol L^{-1} for curves 1 → 5, respectively. The secondary plot represents slope and Y-intercept vs. [myricetin] in the insert, respectively.

Myricetin (structure shown in Fig. 1), a member of the flavonol subclass of flavonoids with antioxidant activities, is commonly distributed in fruits, vegetables, nuts, berries, tea and red wine (Huang et al., 2015). Myricetin was reported to decrease the generation of uric acid and superoxide anion (Cos et al., 1998). However, the investigation was restricted to the enzymatic activity assay, and no report is available on the mechanism of myricetin against XOD. It is essential to clarify the roles of myricetin in inhibiting uric acid formation and O_2^- generation during enzymatic reaction.

The aim of this work was to explore the mechanism of inhibiting O_2^- generation and uric acid formation. Moreover, the binding characteristics of myricetin with XOD and the conformational changes of the enzyme induced by myricetin were characterized by using multispectroscopic methods including UV–vis absorption, fluorescence and circular dichroism (CD) combined with molecular modeling approach.

2. Materials and methods

2.1. Materials

XOD (Grade I, approximately 10.4 units mL^{-1}) from bovine milk and xanthine were purchased from Solarbio Co. (Beijing, China). The stock solutions of XOD (5.0×10^{-6} mol L^{-1}) and xanthine (5.0×10^{-4} mol L^{-1}) were prepared in 0.05 mol L^{-1} Tris–HCl buffer (pH 7.4) for immediate use. Myricetin (analytical grade) was obtained from Aladdin Industrial Co. (Shanghai, China). It was dissolved in absolute ethanol as stock solution (6.0×10^{-3} mol L^{-1}), and then diluted with Tris–HCl buffer as required in experiment process. Both nitroblue tetrazolium (NBT) and phenazine methosulfate (PMS) were purchased from Sinopharm Chemical Reagent Co. (Shanghai, China), and β-NADH (NADH) was provided by Aladdin Chemistry Co. (Shanghai, China). 2,2-Diphenyl-1-picrylhydrazyl (DPPH) was supplied by Sigma–Aldrich Co. (St. Louis, MO) and dissolved in ethanol to the concentration of 3.0×10^{-3} mol L^{-1}. All other reagents and solvents were of analytical reagent grade, and the ultrapure water was used throughout the experiments.

2.2. Assay of uric acid generated by XOD

The inhibition of myricetin on the formation of uric acid was measured using xanthine as the substrate on a Shimadzu UV–2450 spectrophotometer (Shimadzu, Japan) equipped with a 1.0 cm path length cell. A series of 2.0 mL reaction mixture consisting of various amounts of myricetin, Tris–HCl buffer and a fixed concentration of XOD (7.5×10^{-8} mol L^{-1}) were prepared and incubated for 0.5 h at 37 °C. Then the reaction was started by adding substrate xanthine (final concentration 5.0×10^{-5} mol L^{-1}), and the XOD activity was assayed spectrophotometrically by continuously measuring uric acid formation at a wavelength of 290 nm (Tung & Chang, 2010). The relative enzymatic activity (%) = (slope of reaction kinetics equation obtained by reaction with inhibitor)/(slope of reaction kinetics equation obtained by reaction without inhibitor) × 100. Allopurinol was used as a positive control.

2.3. Analysis of inhibitory kinetics

The assay was performed in the absence and presence of myricetin with varying concentrations of xanthine using the same method as the assay of uric acid generated by XOD. Lineweaver–Burk plots in double reciprocal form and the secondary replots were applied to determine the inhibition type of myricetin against XOD. For the mixed-type inhibition, Lineweaver–Burk plots in double reciprocal form can be described by the following equations (Si et al., 2013):

$$\frac{1}{v} = \frac{K_m}{V_{max}}\left(1 + \frac{[I]}{K_i}\right)\frac{1}{[S]} + \frac{1}{V_{max}}\left(1 + \frac{[I]}{\alpha K_i}\right) \quad (1)$$

Secondary plot can be obtained from:

$$\text{Slope} = \frac{K_m}{V_{max}} + \frac{K_m[I]}{V_{max}K_i} \quad (2)$$

and

$$\text{Y} - \text{intercept} = \frac{1}{V_{max}^{app}} = \frac{1}{V_{max}} + \frac{1}{\alpha K_i V_{max}}[I] \quad (3)$$

where K_m and K_i are the Michaelis–Menten constant and inhibition constant, respectively. The enzyme reaction rate is expressed as v in the absence and presence of myricetin. [I] and [S] stand for the concentrations of inhibitor and substrate, respectively. α is the apparent coefficient. If the secondary plot of slope and Y-intercept versus [I] was linearly fitted, it was assumed that only a single inhibition site or a single class of inhibition sites existed (Wang, Zhang, Yan, & Gong, 2014).

2.4. Radical scavenging activity on DPPH radical

The DPPH free radical scavenging activity was determined according to a method as reported previously with slight modification (Fang et al., 2011). Myricetin solution was mixed with 0.66 mL Tris–HCl buffer (pH 7.4), 1.25 mL ethanol and 0.07 mL DPPH. The sample solution was allowed to stand in the dark for 0.5 h, and then its absorbance (A_{sample}) was measured at 517 nm. The absorbance of the control ($A_{control}$) was obtained by replacing myricetin solution with ethanol. The scavenging activity = $[(A_{control} - A_{sample})/A_{control}] \times 100\%$.

2.5. Radical scavenging activity on O_2^- generated by PMS–NADH system

The O_2^- was generated non-enzymatically with a PMS–NADH system. The reaction mixture containing 0.8 mL NBT (1.25×10^{-4} mol L^{-1}), 0.74 mL NADH (7.80×10^{-4} mol L^{-1}) and 0.06 mL myricetin were prepared and incubated at the room temperature for 5 min. Then, the reaction was initiated by adding 0.4 mL PMS solution (1.55×10^{-4} mol L^{-1}) to the mixture and the absorbance at 560 nm was measured for 200 s (Nishikimi, Rao, & Yagi, 1972). 0.06 mL ethanol was used to replace myricetin solution as a control.

2.6. Assay of O_2^- generated by XOD

The O_2^- generated by XOD can reduce NBT to a blue formazan, whose characteristic absorbance was at 560 nm. The test solutions were made by mixing Tris–HCl buffer, XOD (final concentration 2.0×10^{-7} mol L^{-1}) and myricetin in various concentrations. Then the mixtures were incubated for 0.5 h at 37 °C. Afterwards, 0.02 mL NBT (2.5×10^{-3} mol L^{-1}) and 0.04 mL xanthine (0.01 mol L^{-1}) were successively added into the solutions in a total of 2.0 mL, and the absorbance of the mixture at 560 nm was recorded (Masuoka & Kubo, 2004). When the curve shape of the inhibition rate ($iv_i = v_{i=0} - v_i$) vs. [myricetin] is sigmoidal, the inhibition rate was estimated using the Hill equation:

$$Iv_i = v_{i=0}[I]^n/(K_i + [I]^n) \quad (4)$$

where the inhibition rate was a calculated difference between enzymatic reaction rate in the absence of myricetin ($v_{i=0}$) and the rates (v_i) at various concentrations of myricetin. [I] means the concentration of myricetin. n is a slope factor of the sigmoidal curve. K_i is a constant.

2.7. Fluorescence spectra measurements

Fluorescence intensity of the sample was measured using a Hitachi spectrofluorometer model F-7000 (Hitachi, Japan) equipped with a 1.0 cm path-length quartz cell and a circulating water bath. A 2.5 mL of XOD solution (7.0×10^{-7} mol L^{-1}) was titrated by successive additions of myricetin stock solution (0–4.8×10^{-5} mol L^{-1}). The sample solutions were mixed thoroughly and equilibrated before measurements, and then the emission fluorescence was scanned from 300 to 500 nm with the excitation wavelength of 280 nm at four different temperatures (292, 298, 304, and 310 K). The widths of both excitation and emission slits were set at 2.5 nm. The fluorescence data were corrected for the inner-filter effect using the following relationship (Ma, Zhang, & Pan, 2012):

$$F_c = F_m e^{(A_1+A_2)/2} \quad (5)$$

where F_c and F_m denote the corrected and measured fluorescence, respectively. A_1 and A_2 stand for the absorbance of myricetin at excitation and emission wavelengths, respectively. In this work, all the fluorescence intensities used were the corrected fluorescence intensity.

The mechanism of fluorescence quenching can be classified as static, dynamic or a combination of these two processes. The well-known Stern–Volmer equation was used to analyze the fluorescence quenching data to determine the type of fluorescence quenching mode (Zhang, Zhang, Li, & Hu, 2013):

$$\frac{F_0}{F} = 1 + K_{SV}[Q] = 1 + K_q\tau_0[Q] \quad (6)$$

where F_0 and F denote the fluorescence intensities of XOD in the absence and presence of myricetin, respectively. K_{SV} is the Stern–Volmer quenching constant, K_q is the quenching rate constant of the biomolecule ($K_q = K_{SV}/\tau_0$). [Q] represents the concentration of myricetin, τ_0 is the average lifetime (2.80×10^{-9} s) of the fluorophore in the absence of myricetin (Lakowicz & Weber, 1973).

For a static quenching process, the quenching data was estimated using the modified Stern–Volmer equation (Ma et al., 2012):

$$\frac{F_0}{F_0 - F} = \frac{1}{f_a K_a[Q]} + \frac{1}{f_a} \quad (7)$$

where K_a is the modified Stern–Volmer quenching constant for the accessible fluorophores, and f_a is the fraction of accessible fluorescence.

Synchronous fluorescence spectra were measured to study the conformational changes of XOD in the absence and presence of myricetin at 298 K, while $\Delta\lambda$ ($\lambda_{em} - \lambda_{ex}$) was adjusted to 15 nm and 60 nm over a wavelength range of 250–350 nm. The appropriate blank corresponding to the free myricetin and buffer was subtracted to correct for background fluorescence.

2.8. CD tests

A CD spectrometer (Bio-Logic MOS 450, Claix, France) was used to record the CD signal to analyze the structural changes of XOD in aqueous solution induced by the addition of myricetin. The concentration of XOD was fixed at 1.0×10^{-6} mol L^{-1}, and the molar ratios of myricetin to XOD were varied as 0:1, 5:1, 10:1 and 20:1, respectively. All observed CD spectra were measured at room temperature under nitrogen atmosphere with a scan speed of 60 nm min^{-1} and corrected for buffer signal.

2.9. Myricetin–XOD docking simulation

The docking program AutoDock (version 4.2) was used to evaluate the potential interaction between myricetin and XOD. The

crystal structure of XOD from bovine milk (PDB ID: 1FIQ) was taken from the RCSB Protein Data Bank. All the water molecules in XOD were removed, the hydrogen atoms were added and Gasteiger charges were assigned to the PDB file. The 3D structure of myricetin was constructed in Chem3D Ultra 8.0. The dimension of grid maps was set at 126 Å × 126 Å × 126 Å with a grid spacing of 0.375 Å to contain the binding site of XOD as well as significant regions of the surrounding surface (Sui, Zhang, & Zhou, 2016). The grid maps for energy scoring were calculated using AutoGrid. Lamarckian Genetic Algorithm (LGA) was chosen for docking calculations and the search parameters were set to 100 genetic algorithm runs. Other docking parameters were at their default setting. The pose with the lowest binding energy was considered to be the most probable binding mode.

2.10. Statistical analysis

All the tests and analyses were carried out in three replicates. Data were expressed as mean ± standard deviation ($n = 3$) and analyzed by one-way ANOVA using Origin 8.0 software, $p < 0.05$ was considered statistically significant.

3. Results and discussion

3.1. Effects of myricetin on uric acid formation

As shown in Fig. 1A, the activity of XOD was inhibited by myricetin in a concentration-dependent manner. The enzymatic activity decreased to 50% of the initial level when the concentration of myricetin (IC_{50}) reached to $(8.66 \pm 0.03) \times 10^{-6}$ mol L^{-1}, which was slightly higher than that of allopurinol [$(2.69 \pm 0.02) \times 10^{-6}$ mol L^{-1}]. The results indicated that myricetin had a better ability of XOD inhibition. As previously reported (Chang, Lee, Lu, & Chiang, 1992; Wang et al., 2015), kaempferol (4′-OH) and quercetin (3′, 4′-OH) with a similar structure as myricetin (3′, 4′, 5′-OH) more effectively inhibited XOD with IC_{50} values of $(2.18 \pm 0.02) \times 10^{-6}$ mol L^{-1} and 7.23×10^{-6} mol L^{-1}, respectively, suggesting that a number of hydroxyl groups attached to the B-ring may decrease the inhibition on XOD. This may arise from the destabilization of polar hydroxy of benzene ring B stretching into the hydrophobic region of active cavity of XOD and leading to lower binding affinity (Van Hoorn et al., 2002). Plots of v vs. [XOD] at different concentrations of inhibitor were produced (Fig. 1B). All the straight lines passed through the origin and the slopes of the lines were decreased with the increasing concentrations of myricetin, indicating that the inhibition of myricetin on XOD was reversible (Wang, Liu et al., 2014; Wang, Curtis-Long et al., 2014).

3.2. Determination of inhibitory type

The inhibition kinetics was studied based on the Lineweaver-Burk plot (Fig. 1C), and all the data lines with different slopes and intercepts intersected in the second quadrant, indicating that myricetin was a mixed-type inhibitor against the formation of uric acid (Phan, Wang, Tang, Lee, & Ng, 2013). According to the replots of the slope and Y-intercept versus [Myricetin], the values of K_i and α were determined to be $(5.99 \pm 0.03) \times 10^{-6}$ mol L^{-1} and 2.62 ± 0.02 respectively, suggesting that myricetin tended to bind more easily and firmly to the free XOD than to the XOD-xanthine complex (Peng, Zhang, Liao, & Gong, 2016). Furthermore, good linearity was obtained for the secondary plots (inset of Fig. 1C), indicating that myricetin may have a single inhibition site or a single class of inhibition sites on XOD.

3.3. Inhibitory activity on O_2^- generated by XOD

In a two-substrate enzyme system (e.g. XOD reaction), ping-pong mechanism is possible for substrate-enzyme interaction. In brief, it is assumed that XOD has different oxidation states and the fully reduced enzyme contains six electrons in the reduced iron-sulphur center (Hille & Massey, 1981). Then, XOD was divided into oxidised and reduced forms. The oxidised form carries one or two electrons (EI) and catalyses the reaction of oxygen to O_2^-, while the reduced form contains four or six electrons (EII) and involves the reaction of oxygen to hydrogen peroxide (Fig. 2A). Thus, three reactions may be associated with the inhibitory activity of O_2^- generation. (I) Antioxidants suppress the generation of both O_2^- and hydrogen peroxide due to inhibition of uric acid formation; (II) Antioxidants are able to reduce XOD molecules, and the reduced enzyme (EII) only catalyses the formation of hydrogen peroxide; (III) Antioxidants primarily act as reagents of the O_2^- scavenging activity (Masuoka, Matsuda, & Kubo, 2012).

Base on above-mentioned mechanism, the radical scavenging activities on DPPH and the O_2^- generated by the PMS–NADH system were determined. Myricetin exhibited a notable radical scavenging activity of DPPH with the value of (74.68 ± 2.2)% at the concentration of 6.0×10^{-5} mol L^{-1} (data not shown), implying a reduction of the enzyme molecules caused by myricetin. The O_2^- scavenging activity of myricetin was determined to be (56.22 ± 1.2)% at myricetin concentration of 6.0×10^{-5} mol L^{-1} (data not shown), suggesting that myricetin had favourable scavenging activity of O_2^-.

Considering the O_2^- generation catalysed by the enzyme, myricetin inhibited 50% formation of formazan at the concentration of $(4.55 \pm 0.02) \times 10^{-6}$ mol L^{-1}, and the generation of O_2^- decreased

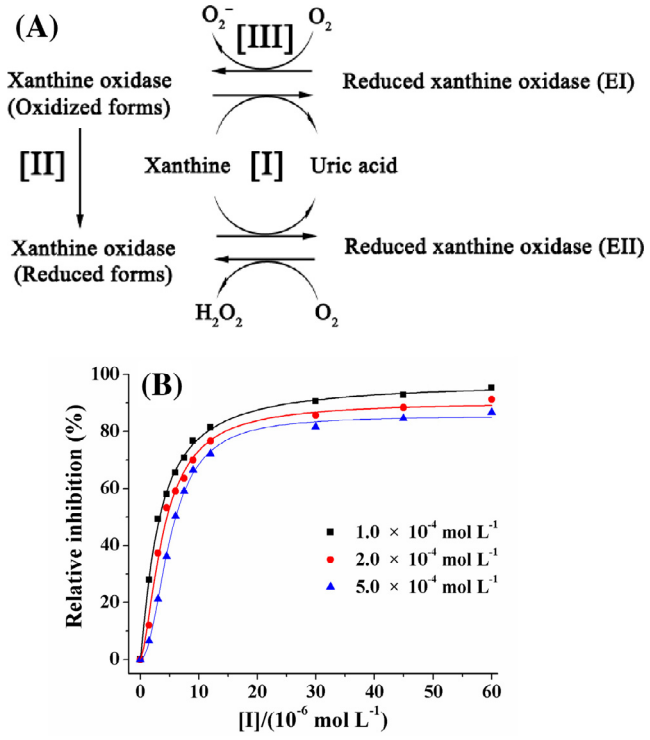

Fig. 2. (A) The ping-pong mechanism for inhibition of the superoxide anion generation catalysed by XOD including three reactions. [I] Inhibition of the XOD reaction with antioxidants. [II] Reduction of the XOD with antioxidants. [III] Scavenging of the superoxide anion with antioxidants. (B) Effects of myricetin on the superoxide anion generated by XOD at three different concentrations of xanthine. c(XOD) = 2.0×10^{-7} mol L^{-1}; c(xanthine) = 1.0, 2.0 and 5.0×10^{-4} mol L^{-1}, respectively.

to 14.3% of the initial level when the concentration of myricetin reached 3.0×10^{-5} mol L^{-1} (Fig. 2B). It should be noted that the inhibition of O_2^- generation by myricetin followed the Hill equation (sigmoidal, $n = 1.58 \pm 0.2$), and the dose–response curve for myricetin was not affected by xanthine concentration, suggesting that myricetin may inhibit the generation of O_2^- catalysed by XOD rather than radical scavenging activity on the O_2^- radicals (Masuoka, Nihei, Maeta, Yamagiwa, & Kubo, 2015). Moreover, the O_2^- scavenging rate of myricetin was low compared to the inhibitory rate of the O_2^- generated by XOD, and myricetin more effectively inhibited the generation of O_2^- than that of uric acid catalysed by XOD. Thus, it was proposed that XOD inhibited by myricetin was ascribed to the reduced form of the enzyme with a substantially higher reduction potential for the FADH./$FADH_2$ couple. One electron can be transferred to the oxygen molecule when oxygen bound to the fully reduced enzyme to form $FADH_2.O_2$ complex. The fully reduced enzyme was regenerated by intramolecular electron from the reduced iron centers and molybdenum and provided another electron to O_2^- to form hydrogen peroxide, leading to the decrease of O_2^- generation (Olson, Ballou, Palmer, & Massey, 1974).

3.4. Fluorescence quenching of XOD by myricetin

Fluorescence quenching is to measure the decrease of the quantum yield of the fluorescence due to molecular interactions such as excited-state reactions, energy transfer, ground-state complex formation, and collisional quenching, which can be used to investigate the interaction between proteins and ligands (Paul, Ray, & Guchhait, 2013). Fig. 3A shows the effect of myricetin on the fluorescence intensity of XOD upon excitation at 280 nm at 298 K. A primary emission peak at 342 nm was exhibited due to the presence of tryptophan and tyrosine in XOD, while insignificant fluorescence peak for myricetin (curve 0) existed at the measured wavelength range. With the increase of myricetin concentrations from 0 to 4.8×10^{-5} mol L^{-1}, the regular decrease in fluorescence intensity of XOD at 342 nm was observed, and there was no distinct shift at the maximum emission wavelength, implying that myricetin may interact with XOD and quench the intrinsic fluorescence of XOD.

As shown in Fig. 3B, the Stern–Volmer plots obtained at different temperatures (292, 298, 304 and 310 K) were linearly fitted, indicating that the fluorescence quenching type was either a static or a dynamic quenching (Paul, Ghosh, & Mukherjee, 2014). An inverse correlation between K_{SV} values and temperatures were observed (Table 1), and the corresponding K_q values reached an order of magnitude of 10^{12}, which were much greater than the maximum diffusion collision quenching rate constant for a biomolecule (2.0×10^{10} L mol^{-1} s^{-1}). Therefore, it can be inferred that the quenching process was mainly governed by a static quenching procedure ascribing to the formation of a ground-state complex.

The K_a values were calculated to be 4.45×10^4 (292 K), 3.24×10^4 (298 K), 2.38×10^4 (304 K) and 1.71×10^4 (310 K) L mol^{-1}, respectively, and the values of K_a decreased with the increase of temperature, which was in agreement with the dependence of K_{SV} on the temperature. The results further indicated that fluorescence quenching process may be predominated by a static quenching mechanism rather than a dynamic procedure.

3.5. Calculation of binding constant and number of binding sites

To characterize the binding properties of myricetin with XOD, and the binding constant and number of binding sites of myricetin-XOD complex can be determined via the Scatchard equation (Barri, Trtic-Petrovic, Karlsson, & Jonsson, 2008):

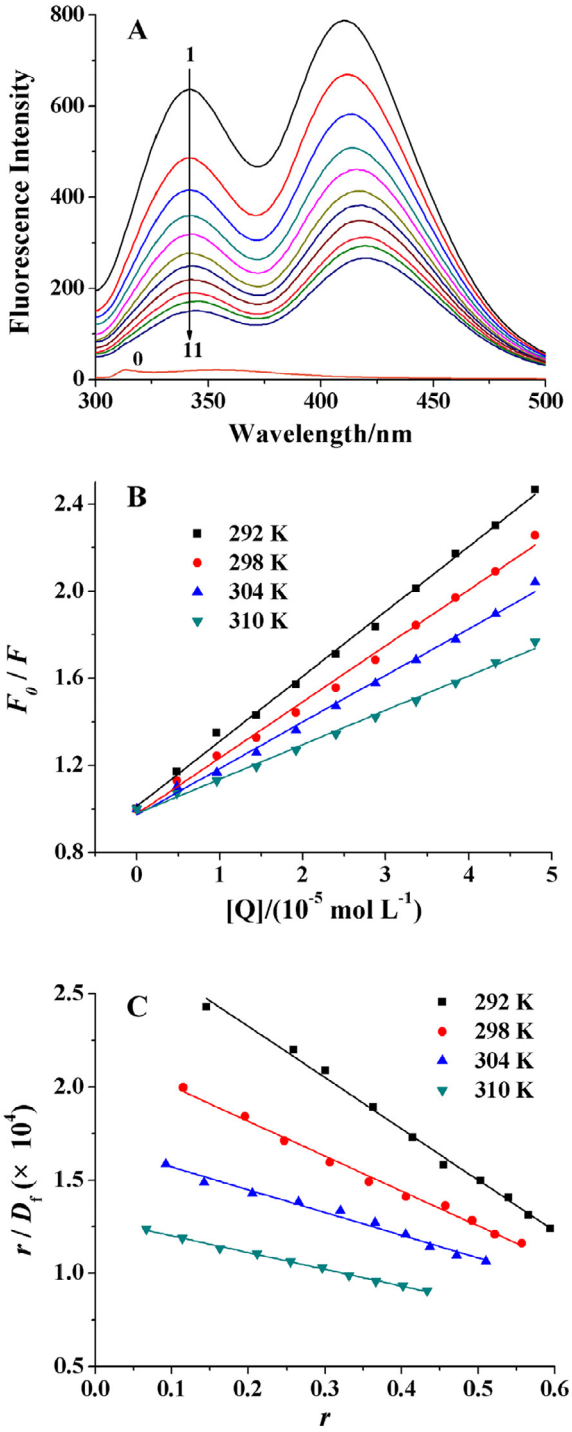

Fig. 3. (A) The fluorescence spectra of XOD in the presence of myricetin at various concentrations. pH 7.4, $T = 298$ K, $\lambda_{ex} = 280$ nm, $\lambda_{em} = 342$ nm. c(XOD) = 7.0×10^{-7} mol L^{-1}; c(myricetin) = 0, 0.48, 0.96, 1.44, 1.92, 2.40, 2.88, 3.36, 3.84, 4.32, and 4.80×10^{-5} mol L^{-1} for curves 1 → 11, respectively. Curve 0 shows the emission spectrum of myricetin only, c(myricetin) = 4.8×10^{-6} mol L^{-1}. (B) The Stern–Volmer plots for the fluorescence quenching of XOD by myricetin at four different temperatures. (C) The Scatchard plots for the myricetin–XOD system.

$$r/D_f = nK_b - rK_b \quad (8)$$

where r is the mole number of myricetin bound per mole of protein, D_f is the molar concentration of free myricetin, n is the number of binding sites per XOD molecule, and K_b means the binding constant.

The Scatchard plots were linearly fitted (Fig. 3C), indicating that myricetin may bind to a class of binding sites on XOD (Paul et al.,

Table 1
The quenching constants (K_{sv}), binding constants (K_b), the number of binding sites (n) and thermodynamic parameters for myricetin–XOD system at different temperatures.

T (K)	K_{SV} ($\times 10^4$ L mol^{-1})	R^a	K_b ($\times 10^4$ L mol^{-1})	R^b	n	ΔH° (kJ mol^{-1})	ΔG° (kJ mol^{-1})	ΔS° (J mol^{-1} K^{-1})
292	2.98 ± 0.01	0.9973	2.75 ± 0.02	0.9944	1.05 ± 0.02	−47.42 ± 0.1	−24.80 ± 0. 1	−77.45 ± 0.2
298	2.57 ± 0.02	0.9949	1.87 ± 0.02	0.9933	1.17 ± 0.03		−24.34 ± 0.1	
304	2.14 ± 0.02	0.9953	1.22 ± 0.03	0.9835	1.39 ± 0.03		−23.88 ± 0.2	
310	1.58 ± 0.02	0.9953	0.90 ± 0.01	0.9967	1.43 ± 0.01		−23.41 ± 0.2	

R^a is the correlation coefficient for the K_{sv} values;
R^b is the correlation coefficient for the K_b values.

2014). The binding constants at the four temperatures were all in the order of magnitude of 10^4 L mol^{-1} (Table 1), suggesting that a moderate affinity existed between myricetin and XOD. Moreover, the binding constants for the system tended to decrease with the increase of temperature, indicating that the binding strength and stability were weakened at a higher temperature (Xie, Wang, Zhou, Wang, & Chen, 2011).

3.6. Thermodynamic analysis and the binding forces

There are four types of non-covalent interaction forces for the ligand-protein binding reactions: hydrophobic interaction, electrostatic interaction, van der Waals force and hydrogen bonds (He & Carter, 1992). Hence, the thermodynamic parameters were determined to characterize the acting forces between myricetin and XOD according to the following equations (Shahabadi, Maghsudi, Kiani, & Pourfoulad, 2011):

$$\lg K_b = -\frac{\Delta H^\circ}{2.303RT} + \frac{\Delta S^\circ}{2.303R} \quad (9)$$

$$\Delta G^\circ = \Delta H^\circ - T\Delta S^\circ \quad (10)$$

where R is the gas constant (8.314 J mol^{-1} K^{-1}), T is the experimental temperature (292, 298, 304 or 310 K) and K_b is the binding constant at corresponding T. ΔH° and ΔS° denote standard enthalpy change and standard entropy change, respectively. ΔG° is free energy change. The calculated thermodynamic parameters for the interaction of myricetin with XOD are summarized in Table 1. The interaction process was spontaneous since the value of ΔG° was negative. Due to the negative value of ΔH°, the binding process was an exothermic reaction so that K_b decreased with the increase of temperature (Table 1). The negative values of ΔH° and ΔS° are frequently regarded as an evidence that the interaction between XOD and myricetin was an enthalpy-driven process, and van der Waals forces and hydrogen bonds dominated the binding process (Ross & Subramanian, 1981).

3.7. Synchronous fluorescence spectroscopy

The synchronous fluorescence was employed to detect the change of the polarity microenvironment around the fluorophores (tyrosine and tryptophan) of XOD when $\Delta\lambda$ was set at 15 nm and 60 nm, respectively. As shown in Fig. 4A, the maximum emission

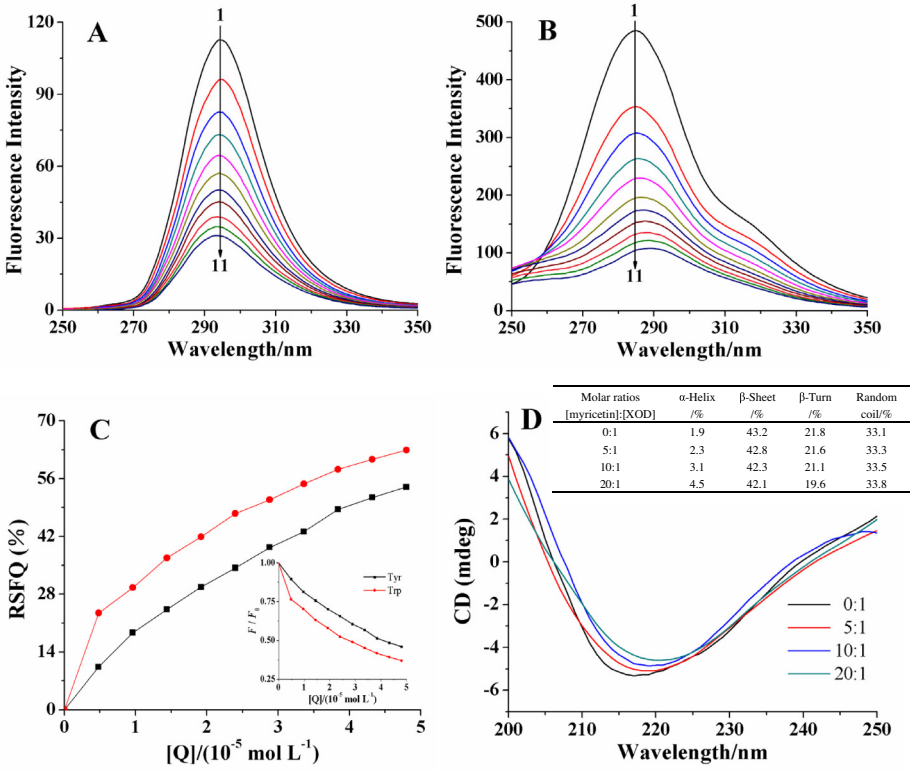

Fig. 4. Synchronous fluorescence spectra of XOD with different concentrations of myricetin at (A) $\Delta\lambda$ = 15 nm and (B) $\Delta\lambda$ = 60 nm. c(XOD) = 7.0 × 10^{-7} mol L^{-1}; c(myricetin) = 0, 0.48, 0.96, 1.44, 1.92, 2.40, 2.88, 3.36, 3.84, 4.32, and 4.80 × 10^{-5} mol L^{-1} for curves 1 → 11, respectively. (C) Comparative evaluation of myricetin effect on the ratios of synchronous fluorescence quenching (RSFQ) of XOD. (D) The CD spectra of XOD in the presence of increasing amounts of myricetin. c(XOD) = 1.0 × 10^{-6} mol L^{-1}; the molar ratios of myricetin to XOD were (1) 0:1, (2) 5:1, (3) 10:1 and (4) 20:1, respectively.

wavelength of tyrosine residue at $\Delta\lambda$ = 15 nm displayed inconspicuous shift upon the addition of myricetin, indicating that the microenvironment around the tyrosine residue had no discernable change. While an obvious red shift (from 285 nm to 289 nm) in the emission spectra at $\Delta\lambda$ = 60 nm was observed (Fig. 4B), which suggested that the hydrophobicity decreased and the polarity increased around the tryptophan residue (Ge et al., 2010).

Moreover, the synchronous fluorescence data was used to calculate the ratios of synchronous fluorescence quenching (RSFQ) of XOD via the equation RSFQ = $1 - F/F_0$, where F and F_0 are the synchronous fluorescence intensities of XOD in the presence and absence of myricetin. The RFSQ values at $\Delta\lambda$ = 60 nm were higher than the corresponding one at $\Delta\lambda$ = 15 nm (Fig. 4C), suggesting that tryptophan residue may make a better contribution to the intrinsic fluorescence quenching and the bound myricetin was nearer to tryptophan than tyrosine residue (Wang, Zhang, & Wang, 2015).

3.8. CD spectra

CD spectra were recorded to study the secondary structure change of XOD induced by myricetin. Only one negative band can be observed at 210–220 nm due to the β-sheet of protein (Wang et al., 2015). Conformational transition of XOD could be traced by the changes in the position and intensity of the bands of CD spectra. When the concentration of myricetin increased, the CD intensity of XOD decreased (shifting to zero) with a slight red shift of the peak (Fig. 4D), suggesting an increase of α-helical content in the protein secondary structure (Yan, Zhang, Hu, & Ma, 2013). The CD spectra data were analyzed by the online SELCON3 program (http://dichroweb.cryst.bbk.ac.uk/html/home.shtml). The β-sheet structure was predominant with a high percentage in XOD (the table in Fig. 4D). With the increasing molar ratios of myricetin to XOD, the α-helical and random coil contents tended to an increase and the β-sheet and β-turn contents tended to decrease, indicating that myticetin induced the secondary structure change of XOD, and thus may have an effect on catalyzing the reaction by the enzyme.

3.9. Molecular simulation

Molecular docking was an available tool to predict the visible combination models between myricetin and XOD. A total of 28 multimember conformational clusters were obtained at a rmsd tolerance of 2.0 Å after the 100 docking runs successfully (Fig. 5A), of which the highest number of the analyzed conformations occurred in the cluster with the lowest binding energy (red histogram in Fig. 5A). Hence, the cluster with the lowest energy (−5.33 kcal mol^{-1}) and the most frequent locus (32 out of 100) was taken as the final model used in the subsequent binding orientation analysis. Besides, the calculated binding Gibbs free energy ($\Delta G_{binding}$ = intermolecular energy + torsional energy) was

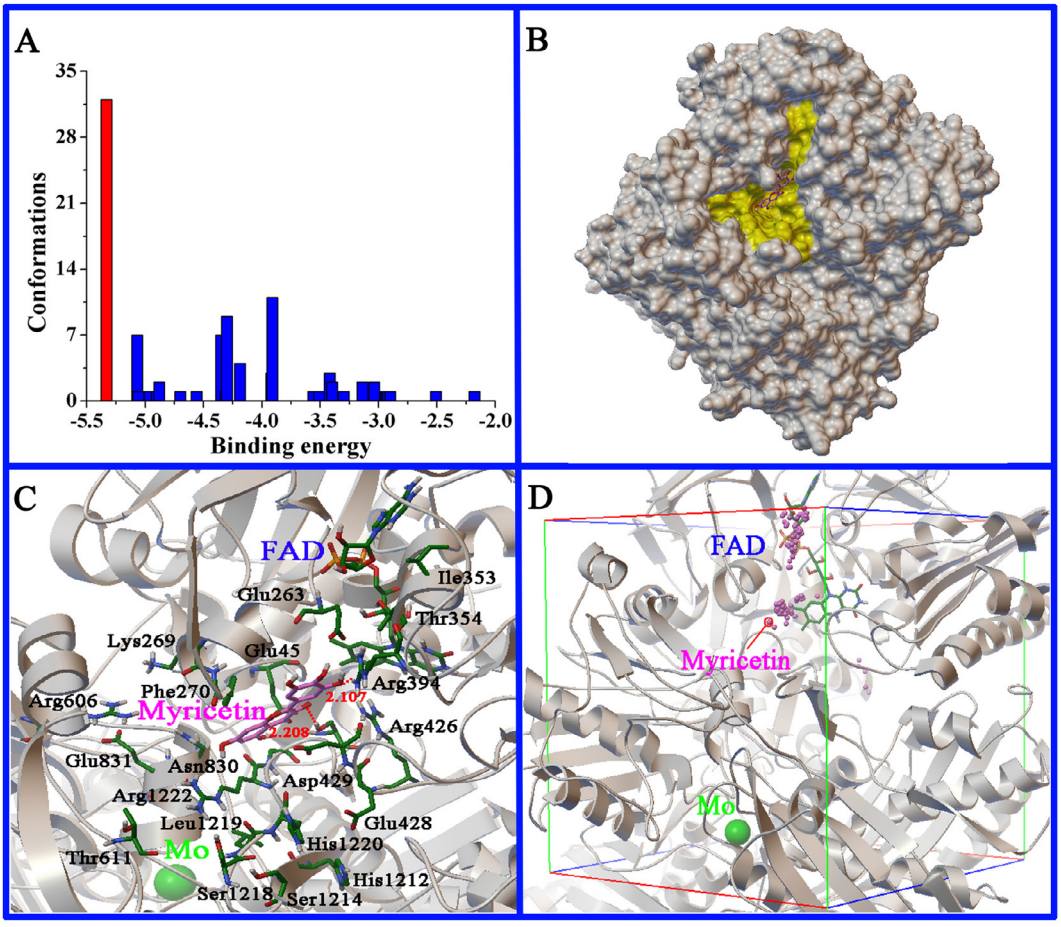

Fig. 5. (A) Cluster analysis of the AutoDock docking runs of myricetin with XOD. (B) The optimal docking form of myricetin in the surface structure (yellow) of XOD. (C) The corresponding close view of myricetin fastening into the active center marked in relative amino acid residues. The hydrogen bonds between myricetin and XOD were marked by red dashed lines. (D) The scatters of myricetin binding to the active cavity of XOD in 100 docking runs. The magenta balls represented the geometrical center of myricetin in each run. (For interpretation of the references to color in this figure legend, the reader is referred to the web version of this article.)

-4.09 kcal mol^{-1}, and the reliability of docking result was confirmed because the result of calculated binding energy was consistent with the predicted binding energy (-4.09 kcal mol^{-1}). The predicted binding energy was slightly higher than the ΔG° (-5.81 kcal mol^{-1}) obtained by above thermodynamic analysis at 298 K, and this may be due to simulation of vacuum environment and the lack of desolvation energy (Wang, Zhang et al., 2014).

Apparently, myricetin had easy access to the active cavity (yellow region, Fig. 5B), where the flavin adenine dinucleotide (FAD) reaction site locates in. Two hydrogen bonds were formed between the oxygen atoms (5′-OH on the B ring and 3-OH on the C ring of myricetin) and the hydrogen atoms on Arg394 and Ser1225 of XOD (Fig. 5C), and their bond lengths were 2.107 and 2.208 Å, respectively, suggesting the involvement of hydrogen bonding in the myricetin–XOD interaction. Fig. 5D displays all the conformational results of myricetin in 100 docking runs, and it was found that the geometrical center of myricetin (magenta ball) in each run was mainly distributed over the isoalloxazine ring in the FAD domain. Thus, it can be inferred that myricetin may bind to the site around isoalloxazine ring in the FAD domain and block the diffusion of O_2^- out of the FAD site, leading to the transfer of another electron from $FADH_2$ to O_2^- to form hydrogen peroxide (Olson, Ballou, Palmer, & Massey, 1974).

4. Conclusions

In summary, myricetin was a reversible mixed-type inhibitor of uric acid formation with an IC_{50} value of $(8.66 \pm 0.03) \times 10^{-6}$ mol L^{-1} and efficiently inhibited the generation of superoxide anion due to the reduced form of the enzyme with a substantially higher reduction potential for the FADH./$FADH_2$ couple. The molecular modeling study validated the experimental results, and confirmed that the inhibition of myricetin on XOD was essentially caused by the binding of myricetin to the isoalloxazine ring in the FAD domain site of XOD, which facilitated the formation of hydrogen peroxide. Van der Waals forces and hydrogen bonds dominated the binding process because the values of ΔH° and ΔS° were -47.42 kJ mol^{-1} and -77.45 J mol^{-1} K^{-1}, respectively. Furthermore, the binding of myricetin to XOD led to the conformational changes with increases in α-helix and random coil contents and decreases in β-sheet and β-turn structure of XOD. Therefore, myricetin may have good future application potential and could be a functional ingredient for food and nutraceutical products to prevent and treat some diseases, such as gout and oxidative damage.

Acknowledgements

This study was supported financially by the National Natural Science Foundation of China (No 31460422), the Natural Science Foundation of Jiangxi Province (20143ACB20006 and 20142BAB204001), and the Objective-Oriented Project of State Key Laboratory of Food Science and Technology (SKLF-ZZA-201612).

References

Barri, T., Trtic-Petrovic, T., Karlsson, M., & Jonsson, J. A. (2008). Characterization of drug-protein binding process by employing equilibrium sampling through hollow-fiber supported liquid membrane and Bjerrum and Scatchard plots. *Journal of Pharmaceutical and Biomedical Analysis, 48*, 49–56.

Chu, Y. H., Chen, C. J., Wu, S. H., & Hsieh, J. F. (2014). Inhibition of xanthine oxidase by Rhodiola crenulata extracts and their phytochemicals. *Journal of Agricultural and Food Chemistry, 62*, 3742–3749.

Cos, P., Ying, L., Calomme, M., Hu, J. P., Cimanga, K., Poel, B. V., ... Berghe, D. V. (1998). Structure activity relationship and classification of flavonoids as inhibitors of xanthine oxidase and superoxide scavengers. *Journal of Natural Products, 61*, 71–76.

Chang, W. S., Lee, Y. J., Lu, F. J., & Chiang, H. C. (1992). Inhibitory effects of flavonoids on xanthine oxidase. *Anticancer research, 13*, 2165–2170.

Enroth, C., Eger, B. T., Okamoto, K., Nishino, T., Nishino, T., & Pai, E. F. (2000). Crystal structures of bovine milk xanthine dehydrogenase and xanthine oxidase: structure-based mechanism of conversion. *Proceedings of the National Academy of Sciences, 97*, 10723–10728.

Fang, J., Yin, H. Z., Liao, L., Qin, H. B., Ueda, F., Uemura, K., ... Maeda, H. (2016). Water soluble PEG-conjugate of xanthine oxidase inhibitor, PEG–AHPP micelles, as a novel therapeutic for ROS related inflammatory bowel diseases. *Journal of Controlled Release, 223*, 188–196.

Fang, R., Hao, R. F., Wu, X., Li, Q., Leng, X. J., & Jing, H. (2011). Bovine serum albumin nanoparticle promotes the stability of quercetin in simulated intestinal fluid. *Journal of Agricultural and Food Chemistry, 59*, 6292–6298.

Ge, F., Chen, C. Y., Liu, D. Q., Han, B. Y., Xiong, X. F., & Zhao, S. L. (2010). Study on the interaction between theasinesin and human serum albumin by fluorescence spectroscopy. *Journal of Luminescence, 130*, 168–173.

Hille, R., & Nishino, T. (1995). Flavoprotein structure and mechanism. 4. Xanthine oxidase and xanthine dehydrogenase. *The FASEB Journal, 9*, 995–1003.

Huang, H., Chen, A. Y., Rojanasakul, Y., Ye, X., Rankin, G. O., & Chen, Y. C. (2015). Dietary compounds galangin and myricetin suppress ovarian cancer cell angiogenesis. *Journal of Functional Foods, 15*, 464–475.

Hille, R., & Massey, V. (1981). Studies on the oxidative half-reaction of xanthine oxidase. *Journal of Biological Chemistry, 256*, 9090–9095.

He, X. M., & Carter, D. C. (1992). Atomic structure and chemistry of human serum albumin. *Nature, 358*, 209–215.

Lakowicz, J. R., & Weber, G. (1973). Quenching of fluorescence by oxygen. Probe for structural fluctuations in macromolecules. *Biochemistry, 12*, 4161–4170.

Masuoka, N., & Kubo, I. (2004). Characterization of xanthine oxidase inhibition by anacardic acids. *Biochimica et Biophysica Acta, 1688*, 245–249.

Ma, Y. D., Zhang, G. W., & Pan, J. H. (2012). Spectroscopic studies of DNA interactions with food colorant indigo carmine with the use of ethidium bromide as a fluorescence probe. *Journal of Agricultural and Food Chemistry, 60*, 10867–10875.

Masuoka, N., Matsuda, M., & Kubo, I. (2012). Characterisation of the antioxidant activity of flavonoids. *Food Chemistry, 131*, 541–545.

Masuoka, N., Nihei, K. I., Maeta, A., Yamagiwa, Y., & Kubo, I. (2015). Inhibitory effects of cardols and related compounds on superoxide anion generation by xanthine oxidase. *Food Chemistry, 166*, 270–274.

Nagao, A., Seki, M., & Kobayashi, H. (1999). Inhibition of xanthine oxidase by flavonoids. *Bioscience, Biotechnology, and Biochemistry, 63*, 1787–1790.

Nishikimi, M., Rao, N. A., & Yagi, K. (1972). The occurrence of superoxide anion in the reaction of reduced phenazine methosulfate and molecular oxygen. *Biochemical and Biophysical Research Communications, 46*, 849–854.

Olson, J. S., Ballou, D. P., Palmer, G., & Massey, V. (1974). The mechanism of action of xanthine oxidase. *Journal of Biological Chemistry, 249*, 4363–4382.

Phan, M. A. T., Wang, J., Tang, J. Y., Lee, Y. Z., & Ng, K. (2013). Evaluation of α-glucosidase inhibition potential of some flavonoids from Epimedium brevicornum. *LWT-Food Science and Technology, 53*, 492–498.

Peng, X., Zhang, G. W., Liao, Y. J., & Gong, D. M. (2016). Inhibitory kinetics and mechanism of kaempferol on α-glucosidase. *Food Chemistry, 190*, 207–215.

Paul, B. K., Ray, D., & Guchhait, N. (2013). Unraveling the binding interaction and kinetics of a prospective anti-HIV drug with a model transport protein: results and challenges. *Physical Chemistry Chemical Physics, 15*, 1275–1287.

Paul, B. K., Ghosh, N., & Mukherjee, S. (2014). Binding interaction of a prospective chemotherapeutic antibacterial drug with β-Lactoglobulin: Results and challenges. *Langmuir, 30*, 5921–5929.

Romano, B., Pagano, E., Montanaro, V., Fortunato, A. L., Milic, N., & Borrelli, F. (2013). Novel insights into the pharmacology of flavonoids. *Phytotherapy Research, 27*, 1588–1596.

Ross, P. D., & Subramanian, S. (1981). Thermodynamics of protein association reactions: Forces contributing to stability. *Biochemistry, 20*, 3096–3102.

Suzuki, H., DeLano, F. A., Parks, D. A., Jamshidi, N., Granger, D. N., Ishii, H., ... Schmid-Schönbein, G. W. (1998). Xanthine oxidase activity associated with arterial blood pressure in spontaneously hypertensive rats. *Proceedings of the National Academy of Sciences, 95*, 4754–4759.

Si, Y. X., Ji, S., Fang, N. Y., Wang, W., Yang, J. M., Qian, G. Y., & Yin, S. J. (2013). Effects of piperonylic acid on tyrosinase: Mixed-type inhibition kinetics and computational simulations. *Process Biochemistry, 48*, 1706–1714.

Sui, X., Zhang, Y., & Zhou, W. (2016). In vitro and in silico studies of the inhibition activity of anthocyanins against porcine pancreatic α-amylase. *Journal of Functional Foods, 21*, 50–57.

Shahabadi, N., Maghsudi, M., Kiani, Z., & Pourfoulad, M. (2011). Multispectroscopicstudies on the interaction of 2-tert-butylhydroquinone (TBHQ), a food additive, with bovine serum albumin. *Food Chemistry, 124*, 1063–1068.

Tung, Y. T., & Chang, S. T. (2010). Inhibition of xanthine oxidase by Acacia confusa extracts and their phytochemicals. *Journal of Agricultural and Food Chemistry, 58*, 781–786.

Van Hoorn, D. E., Nijveldt, R. J., Van Leeuwen, P. A., Hofman, Z., M'Rabet, L., De Bont, D. B., & Van Norren, K. (2002). Accurate prediction of xanthine oxidase inhibition based on the structure of flavonoids. *European Journal of Pharmacology, 451*, 111–118.

Wang, Y. J., Zhang, G. W., Pan, J. H., & Gong, D. M. (2015). Novel insights into the inhibitory mechanism of kaempferol on xanthine oxidase. *Journal of Agricultural and Food Chemistry, 63*, 526–534.

Wang, J., Liu, S., Ma, B., Chen, L., Song, F. R., Liu, Z. Q., & Liu, C. M. (2014). Rapid screening and detection of XOD inhibitors from S. tamariscina by ultrafiltration

LC-PDA-ESI-MS combined with HPCCC. *Analytical and Bioanalytical Chemistry, 406*, 7379–7387.

Wang, Y. J., Zhang, G. W., Yan, J. K., & Gong, D. M. (2014). Inhibitory effect of morin on tyrosinase: Insights from spectroscopic and molecular docking studies. *Food Chemistry, 163*, 226–233.

Wang, Y., Curtis-Long, M. J., Lee, B. W., Yuk, H. J., Kim, D. W., Tan, X. F., & Park, K. H. (2014). Inhibition of tyrosinase activity by polyphenol compounds from Flemingia philippinensis roots. *Bioorganic & Medicinal Chemistry, 22*, 1115–1120.

Wang, Y. P., Zhang, G. W., & Wang, L. H. (2015). Potential toxicity of phthalic acid esters plasticizer: interaction of dimethyl phthalate with trypsin in vitro. *Journal of Agricultural and Food Chemistry, 63*, 75–84.

Xie, X. Y., Wang, Z. W., Zhou, X. M., Wang, X. R., & Chen, X. G. (2011). Study on the interaction of phthalate esters to human serum albumin by steady-state and time-resolved fluorescence and circular dichroism spectroscopy. *Journal of Hazardous Materials, 192*, 1291–1298.

Yan, J. K., Zhang, G. W., Hu, Y. T., & Ma, Y. D. (2013). Effect of luteolin on xanthine oxidase: Inhibition kinetics and interaction mechanism merging with docking simulation. *Food Chemistry, 141*, 3766–3773.

Zhang, Y., Zhang, G. W., Li, Y., & Hu, Y. T. (2013). Probing the binding of insecticide permethrin to calf thymus DNA by spectroscopic techniques merging with chemometrics method. *Journal of Agricultural and Food Chemistry, 61*, 2638–2647.